AD NUMBER
ADB374970
LIMITATION CHANGES
TO: **Approved for public release; distribution is unlimited.**
FROM: **Distribution authorized to U.S. Gov't. agencies and their contractors; Administrative/Operational Use; 23 NOV 2011. Other requests shall be referred to Air Force Research Laboratory, ATTN: AFRL/RXQO, 139 Barnes Drive, Suite 2, Tyndall AFB, FL 32403-5323.**
AUTHORITY
Public Affairs Case No. 88ABW-2011-6234, 2 Dec 2011

AFRL-RX-TY-TR-2011-0061

SUPEROLEOPHOBIC TEXTILES

Hoon Joo Lee, Stephen Michielsen, Colin Willis, Corinne Stone, Jimmei Du, Euigyoung Jeong, Duyanada Satan and Rahul Saraf

North Carolina State University
2401 Research Drive
Raleigh, NC 27695-8301

Contract No. FA8650-07-1-5916

June 2011

.

AIR FORCE RESEARCH LABORATORY
MATERIALS AND MANUFACTURING DIRECTORATE

■ **Air Force Materiel Command** ■ **United States Air Force** ■ **Tyndall Air Force Base, FL 32403-5323**

DISCLAIMER

Reference herein to any specific commercial product, process, or service by trade name, trademark, manufacturer, or otherwise does not constitute or imply its endorsement, recommendation, or approval by the United States Air Force. The views and opinions of authors expressed herein do not necessarily state or reflect those of the United States Air Force.

This report was prepared as an account of work sponsored by the United States Air Force. Neither the United States Air Force, nor any of its employees, makes any warranty, expressed or implied, or assumes any legal liability or responsibility for the accuracy, completeness, or usefulness of any information, apparatus, product, or process disclosed, or represents that its use would not infringe privately owned rights.

NOTICE AND SIGNATURE PAGE

Using Government drawings, specifications, or other data included in this document for any purpose other than Government procurement does not in any way obligate the U.S. Government. The fact that the Government formulated or supplied the drawings, specifications, or other data does not license the holder or any other person or corporation; or convey any rights or permission to manufacture, use, or sell any patented invention that may relate to them.

This report was cleared for public release by the 88th Air Base Wing Public Affairs Office at Wright Patterson Air Force Base, Ohio and is available to the general public, including foreign nationals. Copies may be obtained from the Defense Technical Information Center (DTIC) (http://www.dtic.mil).

AFRL-RX-TY-TR-2011-0061 HAS BEEN REVIEWED AND IS APPROVED FOR PUBLICATION IN ACCORDANCE WITH ASSIGNED DISTRIBUTION STATEMENT.

OWENS.JEFFERY.RAY.1235753983 Digitally signed by OWENS.JEFFERY.RAY.1235753983 DN: c=US, o=U.S. Government, ou=DoD, ou=PKI, ou=USAF, cn=OWENS.JEFFERY.RAY.1235753983 Date: 2011.08.30 10:10:19 -05'00'

JEFFERY R. OWENS, PhD
Work Unit Manager

HENLEY.MICHAEL.V.1231823332 Digitally signed by HENLEY.MICHAEL.V.1231823332 DN: c=US, o=U.S. Government, ou=DoD, ou=PKI, ou=USAF, cn=HENLEY.MICHAEL.V.1231823332 Date: 2011.10.12 09:15:48 -05'00'

MICHAEL V. HENLEY, DR-III
Chief, Airbase Sciences Branch

RHODES.ALBERT.N.III.1175488622 Digitally signed by RHODES.ALBERT.N.III.1175488622 DN: c=US, o=U.S. Government, ou=DoD, ou=PKI, ou=USAF, cn=RHODES.ALBERT.N.III.1175488622 Date: 2011.11.23 08:21:59 -06'00'

ALBERT N. RHODES, PhD
Chief, Airbase Technologies Division

This report is published in the interest of scientific and technical information exchange, and its publication does not constitute the Government's approval or disapproval of its ideas or findings.

REPORT DOCUMENTATION PAGE

Form Approved
OMB No. 0704-0188

PLEASE DO NOT RETURN YOUR FORM TO THE ABOVE ADDRESS.

1. REPORT DATE *(DD-MM-YYYY)*	2. REPORT TYPE	3. DATES COVERED *(From - To)*
19-JUN-2011	Final Technical Report	01-MAY-2007 -- 20-JUN-2011

4. TITLE AND SUBTITLE

Superoleophobic Textiles

5a. CONTRACT NUMBER

5b. GRANT NUMBER

FA8650-07-1-5916

5c. PROGRAM ELEMENT NUMBER

6. AUTHOR(S)

Lee, Hoon Joo; Michielsen, Stephen; Willis, Colin; Stone, Corinne; Du, Jinmei; Jeong, Euigyoung; Satam, Dnyanada; Saraf, Rahul

5d. PROJECT NUMBER

5e. TASK NUMBER

5f. WORK UNIT NUMBER

QL102006

7. PERFORMING ORGANIZATION NAME(S) AND ADDRESS(ES)

North Carolina State University
2401 Research Drive
Raleigh, NC 27695-8301

8. PERFORMING ORGANIZATION REPORT NUMBER

9. SPONSORING/MONITORING AGENCY NAME(S) AND ADDRESS(ES)

Air Force Research Laboratory
Materials and Manufacturing Directorate
Airbase Technologies Division
139 Barnes Drive, Suite 2
Tyndall Air Force Base, FL 32403-5323

10. SPONSOR/MONITOR'S ACRONYM(S)

AFRL/RXQL

11. SPONSOR/MONITOR'S REPORT NUMBER(S)

AFRL-RX-TY-TR-2011-0061

12. DISTRIBUTION/AVAILABILITY STATEMENT

Distribution Statement A: Approved for public release; distribution unlimited.

13. SUPPLEMENTARY NOTES

Ref Public Affairs Case # 88ABW-2011-6234, 2 December 2011. Document contains color images.

14. ABSTRACT

A superoleophobic surface has been achieved by modeling surface morphology and reducing surface energy. A meta-stable Cassie -Baxter model, which describes the transition from a Cassie -Baxter surface to a Wenzel surface caused by the local minimization of surface free energy due to air pockets inside the rough structure, has been used to account for the superoleophobic effect. Under the guidance of AFRL, Natick Soldier RD&EC, and Defense Science and Technology Laboratory (Dstl), we have explored three different techniques to achieve superhydrophobicity and superoleophobicity using nylon/cotton woven fabric (nyco) and hydroentangled nylon nonwoven fabric: pulsed plasma polymerization of fluorodecyl acrylate (PFAC8), microwave-assisted condensation of perfluorodecyltrimethoxysilane (FS), and FS condensation through wet processing. Fabric materials prepared using these three techniques were superhydrophobic and superoleophobic as shown by their very high contact angles for both water and oils. The measured contact angles agree with the predicted values obtained through designing a Cassie-Baxter surface.

15. SUBJECT TERMS

superhydrophobic, superoleophobic, textiles

16. SECURITY CLASSIFICATION OF:			17. LIMITATION OF ABSTRACT	18. NUMBER OF PAGES	19a. NAME OF RESPONSIBLE PERSON
a. REPORT	b. ABSTRACT	c. THIS PAGE			Jeffery R. Owens
U	U	U	UU	38	19b. TELEPHONE NUMBER *(Include area code)*

Reset

Standard Form 298 (Rev. 8/98)
Prescribed by ANSI Std. Z39.18

TABLE OF CONTENTS

LIST OF FIGURES

LIST OF TABLES

Table **Page**

1. SUMMARY

A superoleophobic surface has been achieved by modeling surface morphology and reducing surface energy. A metastable (MS) Cassie–Baxter (CB) model, which describes the transition from a CB surface to a Wenzel surface caused by the local minimization of surface free energy due to air pockets inside the rough structure, has been used to account for the superoleophobic effect. Under the guidance of Air Force Research Laboratory (AFRL), Natick Soldier Research, Development, and Engineering Center (RD&EC), and UK Defense Science and Technology Laboratory (Dstl), we have explored three different techniques to achieve superhydrophobicity and superoleophobicity using a nylon–cotton woven fabric (NyCo) and hydroentangled nylon (HN) nonwoven fabric (HNF): pulsed plasma polymerization of 1H,1H,2H,2H-perfluorodecyl acrylate (PFAC8), microwave-assisted condensation of 1H,1H,2H,2H-perfluorodecyltrimethoxysilane (FS), and FS condensation through wet processing. Fabric materials prepared using these three techniques were superhydrophobic and superoleophobic as shown by their very high contact angles for both water and oils. The measured contact angles agree with the predicted values obtained through designing a CB surface.

2. INTRODUCTION

Technologies related to superhydrophobic and superoleophobic treatments have recently attracted considerable attention in the textile industry due to their potential applications in medical devices as well as industrial materials. A surface whose water contact angle exceds150° is called a *superhydrophobic* surface, and we define a surface with an oil contact angle larger than 150° a *superoleophobic* surface. As the wettability of a solid surface is determined by two parameters, the chemical composition and the geometrical structure of a rough surface, the combination of these two factors is often used to design superhydrophobic and superoleophobic textiles. More specifically researchers employ two predominant rough surface wetting models, the Wenzel model and the CB model compared to the wetting behavior of a smooth surface, to predict the requirements for imparting superhydrophobic and superoleophobic character to a fabric. However, not all surfaces having high contact angles to liquids possess low roll-off angles. Rather, roll-off angles are highly dependent on the mass and density of the droplet, the surface tensions of both the liquid and the surface the droplet is sitting atop, and the geometrical morphology and degree of roughness of that surface. Typically, unless a surface possesses a very low surface tension that is approximately one forth the surface tension of the liquid, droplets of less than 50 μL are not mobile when the surface is tilted.

First, the relationships amongst contact angles, surface tension and surface roughness are reviewed; the wetting behavior of a rough surface is compared with that of a smooth surface; the relationships between contact angle hysteresis and roll-off angles are analyzed, and finally a superhydrophobic, superoleophobic woven fabric is designed and developed using chemical and geometrical surface modifications. Later, we design and prepare superhydrophobic/superoleo-phobic/anti-icing HNFs. Nylon is naturally hydrophilic, so it is essential that the surface be treated with hydrophobic materials to offset the hydrophilicity of nylon. The $–NH_2$ end groups present in nylon facilitate dyeing and finishing of the nonwoven fabric. We report on three chemical modification techniques as approaches for making superoleophobic HNFs: (a) PFAC8, (b) microwave-assisted grafting of FS nanoparticles, and (c) FS grafting via wet processing. Attaching these fluorochemicals to surfaces should reduce the surface energy of the fabric and will potentially generate superhydrophobic and superoleophobic materials. Finally, we determine the anti-icing property of superhydrophobic/superoleophobic surfaces. The anti-icing behavior depends on the surface morphology as well as the surface tension of the substrate. This implies that both the chemistry and the morphology of the anti-icing coating material is important; therefore, the relationship between the anti-icing property and the morphology of a superhydrophobic surface should be studied further. Preliminary results indicate that protective gear that is superhydrophobic could provide substantial reduction in the logistics associated with de-icing.

3. METHODS, ASSUMPTIONS, AND PROCEDURES

3.1. Materials

Nylon 6,6 film (M_n: 12 kDa, Dupont Canada), NyCo, and HNF (Nonwoven Institute, NCSU) were used as the smooth and rough surfaces, respectively. FS ($C_8F_{17}CH_2CH_2Si(OCH_3)_3$, Gelest), PFAC8 ($C_8F_{17}CH_2CH_2OCOCH{=}CH_2$, Fluorochem, Derbyshire, UK), tetramethyl orthosilicate (TMOS, $Si(OCH_3)_4$, Aldrich), ammonium hydroxide (NH_4OH, Mallinckrodt Chemical, Raleigh, NC, USA), methanol (CH_3OH, Aldrich), isopropyl alcohol (C_3H_7OH, Fisher), poly(acrylic acid), ((PAA), $(C_3H_4O_2)_n$, Aldrich), ethylene diamine (EDA) $H_2NCH_2CH_2NH_2$, Aldrich), 4-(4, 6-dimethoxy-1, 3, 5-triazin-2-yl)-4-methylmorpholinium chloride (DMTMM, Aldrich), and hydrogen chloride (HCl, Aldrich) were used without further purification. Distilled water (NCSU) and dodecane ($C_{12}H_{26}$, Aldrich) were used for contact angle measurements.

3.2. Pulse Plasma Polymerization of PFAC8

The grafting of PFAC8 onto nylon 6,6 film and onto a 100 g/m^2 nylon nonwoven substrate was carried out in a cylindrical, inductively-coupled plasma reactor (10 cm diameter and 2700 cm^3 volume) housed in a heated Perspex® chamber. Internal pressure was measured using a thermo-couple pressure gauge. Prior to each experiment, the reactor was cleaned with an air plasma run at 50 W for at least 30 min. The system was pumped back down to base pressure (typically lower than 1×10^{-2} mbar) before being raised to 1 atm to allow insertion of the sample (approximately 12 cm × 20 cm). The sample was placed on a glass shelf situated within the length of the external radio frequency (RF) coil (10 turns, center tapped, outside diameter 12 cm). An L–C matching unit was used to minimize the standing wave ratio of the transmitted power between the 13.56-MHz RF generator and the electrical discharge. An RF probe and oscilloscope were used to monitor the RF pulse width produced by a pulse generator. PFAC8 (2 mL) was placed in a monomer tube attached to the air inlet side of the reactor and purified by freeze–thaw cycling prior to use. All connections were grease free.

While the reactor was pumping down, heaters were turned on and the whole reactor (including the monomer tube) was heated to 34 °C. Once base pressure had been reached, the monomer was bled into the reactor through a Young's tap to a pressure of approximately 1×10^{-1} mbar, and maintained at this pressure. The monomer vapor was allowed to purge through the reactor for 2 min before the plasma was ignited. Once ignited the plasma was run as a continuous wave plasma (30 W) for 30 sec to deposit a priming layer to improve adhesion. After 30 sec, the pulse generator was switched on and a pulsed plasma polymer deposition carried out for 20 min using a stable pulse envelope as indicated by the oscilloscope.

A typical pulse sequence used was 40 µs on 20 ms off. After the plasma treatment, the monomer vapor was allowed to purge through the reactor for an additional 2 min before the system was isolated from the monomer vapor and pumped down to base pressure. Once base pressure was reached, the plasma chamber was slowly raised to atmospheric pressure, and the samples were removed.

3.3. Microwave-assisted Grafting of FS

In the microwave-assisted grafting, FS was partially condensed prior to treating a nylon nonwoven fabric or NyCo woven fabric. A 1-mL portion of 1% aqueous ammonium hydroxide solution was added to 9 mL of a 4% solution of FS in isopropyl alcohol. A 10-cm × 10-cm strip of HNF or NyCo woven fabric was immersed in this solution and then padded to remove excess liquid, yielding approximately 80% (w/w) wet pick-up and cured in a microwave oven (Panasonic NN-SD967S) at 2.45 GHz, 1.25 kW for 30 sec. The FS-grafted fabrics were sonicated in isopropyl alcohol for 10 min, rinsed with water for 30 min and air dried.

3.4. Grafting FS through Wet Processing

A 4 g/L aqueous solution of PAA was prepared with continuous stirring. A 20-cm × 20-cm piece of nylon 6,6 film (Dupont Canada) and a 20-cm x 20-cm piece of HNF were immersed, padded, and cured at 150 °C for 5 min to graft PAA onto them. The PAA-grafted fabric was then immersed in a 4 g/L EDA aqueous solution for 24 hr with continuous shaking. After 24 hr, 0.5 g DMTMM in 10 mL of methanol was added to the mixture and the reaction was allowed to proceed for 2 hr. The fabric was washed with methanol for 8 hr. The EDA-g-PAA-g-nylon fabrics were drawn and padded through dilute HCl solution (0.1 M) and dried at 100 °C for 2 min. The fabrics were rinsed with tap water and dried at room temperature.

Next, a 10% w/w solution of FS in methanol was prepared. The prepared fabrics were drawn and padded through the solution at 100% wet pick-up and dried at 100 °C for 2 min. The fabrics were drawn and padded through the FS solution a second time. The zero-time control fabric was immediately cured at 150 °C for 5 min while the other fabrics were allowed to cure for 2 hr.

3.5. Scanning Electron Microscopy

The nylon nonwoven fabric was examined using a scanning electron microscope (SEM, Hitachi S-3200N) operated at 5 and 10 kV and magnifications from ×50 to ×50,000. Revolution™ v1.60b24 (4pi Analysis Inc.) was used for image analysis of SEM images. The fiber diameters and the distances between adjacent fibers were measured. Each sample was observed at five or more different places at random.

3.6. Contact Angle Measurements

The contact angles of water and dodecane on the treated surfaces were measured by the sessile drop method, using a lab-designed goniometer at 20 °C. The volume of each deposited droplet was 10 μL. The range of contact angles was obtained from at least three individual measurements, each on a new spot. The image of liquid droplets on the prepared surface was obtained using a digital camera (Cannon EOS EF-S-18-55IS) attached to a stereo microscope (Meiji Techno EMZ-13TR).

3.7. Roll-off Angle Measurements

Roll-off angles were measured by placing a specimen on a level platform mounted on a Newport 495 rotation stage and inclining the specimen. Drops (50 μL) of water or dodecane were placed on the surface, the stage was rotated and the angle of the stage was recorded when each drop rolled off. The range of roll-off angles was measured at five different spots on the fabric.

3.8. Anti-icing Characteristics Assessment

A bottled mineral water (Nestle™) was kept in the freezer at -18 °C for 2 hr, ensuring that it did not freeze. The supercooled water was then dropped on inclined (50°) nylon nonwoven fabrics that were frozen for the same amount of time as the fabrics. This was done to freeze the fabric and any atmospheric moisture present in the fabric. These conditions simulate a fabric worn in the winter subject to freezing rain or sleet. Immediately after removing the water and fabric from the freezer, the water was poured onto the fabric surface.

4. RESULTS AND DISCUSSION

4.1. Wetting Behavior of Smooth and Rough Surfaces

Although it is hard to measure the surface tension of a solid directly, it is easy to measure the contact angles of liquid droplets sitting atop its surface (Fig. 1). By obtaining contact angle data for liquids with varying surface tensions and inserting the data into select equations predictions of a surface's wetting characteristics to other liquids can be obtained.

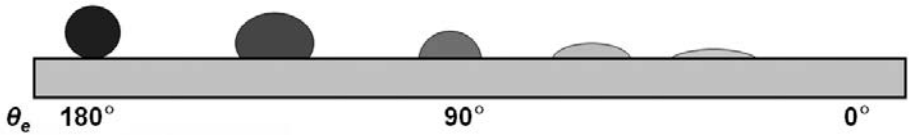

Figure 1. Contact Angle and Wettability

The relationship between surface tension and contact angle is obtained by the Young equation:

$$\frac{\gamma_{SV} - \gamma_{SL}}{\gamma_{LV}} = \cos\theta_e \tag{1}$$

where γ is the surface tension; and subscripts SV, SL, and LV indicate the solid–vapor, the solid–liquid, and the liquid–vapor interfaces, respectively (Fig. 2). According to Young's equation, the contact angle is a well-defined property that depends on the surface tension coefficients that exist between the solid−liquid and the liquid−gas interfaces.

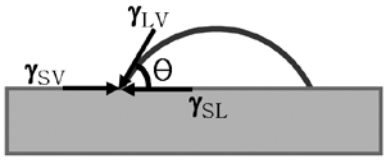

Figure 2. Drop on a Flat Surface

The right hand side of Equation 1 and γ_{LV} can be obtained from experimental measurements, leaving two unknowns, γ_{SV} and γ_{SL}. When θ_e for a test liquid is> 20°, it is assumed that $\gamma_{SV} \approx \gamma_S$ and $\gamma_{LV} \approx \gamma_L$. On the other hand, the thermodynamic work of adhesion, W_{SL}^a can be explained by the Dupre equation as:

$$W_{SL}^a = \gamma_{SV}^a + \gamma_{LV}^a - \gamma_{SL}^a \tag{2}$$

Combining Equations 1 and 2 results in the Dupre–Young equation:

$$W_{SL}^a = \gamma_{SV}^a + \gamma_{LV}^a - \gamma_{SL}^a = \gamma_{LV}^a(1 + \cos\theta_e) \tag{3}$$

According to Fowkes, when only dispersion interactions are present, the interfacial tension between the solid and liquid is $\gamma_{SL}^{LW} = (\sqrt{\gamma_{SV}^{LW}} - \sqrt{\gamma_{LV}^{LW}})^2$ and the geometric mean of the liquid and solid surface tension is

$$W_{SL}^{LW} = 2\sqrt{\gamma_{SV}^{LW}\gamma_{LV}^{LW}} \tag{4}$$

where $W_{SL}{}^{LW}$ is the thermodynamic work of Lifshitz–van der Waals (LW) components.

Meanwhile, the addition of intermolecular forces at the interface is equal to the surface tension of the material, as shown in Equation 5.

$$\gamma = \gamma^{d} + \gamma^{p} + \gamma^{H} + \gamma^{ind} + \gamma^{m} + ... \tag{5}$$

where d, p, H, ind, and m mean London dispersion forces, permanent dipoles, hydrogen bonds, induced dipoles and metallic interaction, respectively. Therefore, we can determine γ_{SV} and γ_{LV} as

$$\gamma_{SV} = \gamma_{SV}^{d} + \gamma_{SV}^{p} + \gamma_{SV}^{H} + \gamma_{SV}^{ind} + \gamma_{SV}^{m} + ... \tag{6}$$

$$\gamma_{LV} = \gamma_{LV}^{d} + \gamma_{LV}^{p} + \gamma_{LV}^{H} + \gamma_{LV}^{ind} + \gamma_{LV}^{m} + ... \tag{7}$$

Combining Equations 3, 4, 6, and 7 gives

$$\begin{aligned} &\gamma_{LV}(1+\cos\theta_e) \\ &= \gamma_{LV}^{d}(1+\cos\theta_e) + \gamma_{LV}^{p}(1+\cos\theta_e) + \gamma_{LV}^{H}(1+\cos\theta_e) + \gamma_{LV}^{ind}(1+\cos\theta_e) + \gamma_{LV}^{m}(1+\cos\theta_e) + ... \\ &= 2(\sqrt{\gamma_{SV}^{d}\cdot\gamma_{LV}^{d}} + \sqrt{\gamma_{SV}^{p}\cdot\gamma_{LV}^{p}} + \sqrt{\gamma_{SV}^{H}\cdot\gamma_{LV}^{H}} + \sqrt{\gamma_{SV}^{ind}\cdot\gamma_{LV}^{ind}} + \sqrt{\gamma_{SV}^{m}\cdot\gamma_{LV}^{m}} + ...) \end{aligned} \tag{8}$$

Since the surface tensions of dodecane and most polymeric surfaces are determined by London dispersion forces, this equation can be simplified to

$$\gamma_{LV}(1+\cos\ \theta_e) = 2(\sqrt{\gamma_{SV}^{d}\cdot\gamma_{LV}^{d}}) \tag{9}$$

An oil such as dodecane has a very low surface tension, ~24.5 dyne/cm. Substituting γ_{LV} = 24.5 dyne/cm for dodecane into Equation 9 suggests γ_{SV} must be smaller than 6.3 dyne/cm, and a smooth surface having $\gamma_{SV} \leq 6.3$ dyne/cm is oleophobic ($\theta_e > 90^o$) under these conditions. The Young equation and Dupre–Young equation are valid only for the wetting of smooth surfaces, but real solids are not perfectly flat and surface structure greatly affects wettability, e.g., when a rough surface of a solid is very hydrophobic, liquid droplets are in contact with the upper part of a rough surface and the lower part is filled with air.

To design a superhydrophobic superoleophobic surface, two predominant rough wetting models are used: the Wenzel model and the CB model. In the Wenzel model a liquid fills the grooves of a rough surface and completely wets the surface, while in the CB model, a liquid sits on top of

the surface and repels the liquid. To create a CB surface, the Young contact angle of a liquid, θ_e, must be greater than 90º, as shown in Figure 3.

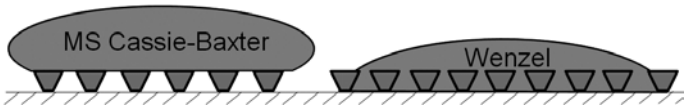

Figure 3. Drop on a Rough Surface

In Wenzel's approach the liquid fills the grooves on the rough surface, and the liquid contact angle on a rough surface, θ_r^W, can be described as

$$\cos\theta_r^{\,W} = r\cos\theta_e \tag{10}$$

where r is roughness — the ratio of the total wet area of a rough surface to the apparent surface area in contact with the water droplet ($r > 1$). According to Equation 10, a hydrophilic rough ($r > 1$) surface becomes more hydrophilic and a hydrophobic rough surface grows more hydrophobic — e.g., for a material with $\theta_e \approx 120º$, r must be greater than 1.79 to make the surface superhydrophobic. Since most solid surfaces typically possess $\gamma_{SV} > 6.3$ dyne/cm, the CB model does not allow for stable superoleophobicity under normal circumstances. On a MS CB surface, a liquid initially sits atop the surface because air pockets inside the grooves of the rough surface provide lower Gibbs free energy than that when the liquid penetrates the rough surface. However, the liquid can be potentially drawn into contact with the rough surface over time, with the time to absorption dependent on the surface tension, volume and density of the liquid, and the surface tension and morphology of the surface. Hence, a superoleophobic surface can be produced by designing a MS CB surface.

The C B model is a form of the Wenzel model extended to include porous surfaces. In this model a liquid sits on a composite surface made of a solid and air. Therefore, the liquid does not fill the grooves of a rough solid. In their paper published in 1944, Cassie and Baxter suggested that the liquid contact angle at on such a rough surface, θ_r^{CB}, is

$$\cos\theta_r^{\,CB} = f_1\cos\theta_e - f_2 \tag{11}$$

where f_1 is the surface area of the liquid in contact with the solid divided by the projected area, and f_2 is the surface area of the liquid in contact with air trapped in the pores of the rough surface divided by the projected area. When there is no trapped air, f_1 is the same as r in the Wenzel model. In the CB model, the smooth surface can become more hydrophobic or oleophobic by surface roughening, regardless of θ_e. However, in the Wenzel model, θ_e has to be greater than 90º for a smooth surface to be more hydrophobic or oleophobic after roughening. This statement reinforces the concept of the MS CB model, i.e., a surface having $\theta_e < 90º$ with a liquid, when roughened, will immediately wet (Wenzel behavior) or the liquid will sit on top of the surface due to air pockets inside the grooves, which results in a local minimum in the surface energy (MS CB behavior). In addition, as the surface tension of an oil such as dodecane is lower than that of water ($\gamma = 72.8$ dyne/cm), θ_r^{CB} of water is higher than θ_r^{CB} of oil. Hence, according to

Equations 10 and 11, all superoleophobic surfaces should be superhydrophobic, but not all superhydrophobic surfaces exhibit superoleophobicity.

4.2. Modeling of Self-cleaning Surfaces

Superhydrophobicity has gained a great deal of interest and has been studied extensively since one of the most-prized features of superhydrophobic surfaces is their ability to self-clean—that is that water collects and removes dirt and debris as the water droplet rolls off the surface. The roll-off angle of a droplet, α, on a smooth surface can be described as

$$mg\sin\alpha \approx -2R_w\gamma_{LV}(\cos\theta_A - \cos\theta_R) \tag{12}$$

where m is the mass of the droplet, V is the volume of the droplet, g is the gravitational acceleration, R_w is the radius of the wetting area, θ_A is the advancing contact angle, and θ_R is the receding contact angle. Meanwhile, contact angle hysteresis, $\Delta\theta_H$, is defined as the difference between advancing and receding contact angles, i.e. $\Delta\theta_H = \theta_A - \theta_R$. The gain factor, which is often used to understand the relationship between contact angle hysteresis and roll-off angle, is reckoned as the rate of variation of the contact angle hysteresis at any operating point. The radius of the wetting area, R_w, on a surface is

$$R_w = \sqrt[3]{\frac{3V}{\pi(2-3\cos\theta+\cos^3\theta)}}\sin\theta \tag{13}$$

Based on Equation 13, the radius of the wetting area can be predicted as shown in Table 1.

Table 1. Measured Radius of Wetting Area of Liquid Droplets

θ (°)	R_c (mm)			
	5μL	10 μL	20 μL	50 μL
10	3.31	4.17	5.26	7.14
20	2.62	3.30	4.15	5.63
30	2.27	2.85	3.60	4.88
40	2.03	2.56	3.23	4.38
50	1.86	2.34	2.94	4.00
60	1.71	2.15	2.71	3.68
70	1.58	1.99	2.50	3.40
80	1.46	1.83	2.31	3.13
90	1.34	1.69	2.12	2.88
100	1.22	1.54	1.94	2.63
110	1.10	1.39	1.75	2.37
120	0.97	1.23	1.55	2.10
130	0.84	1.06	1.33	1.81
140	0.69	0.87	1.10	1.49
150	0.54	0.67	0.85	1.15
160	0.37	0.46	0.58	0.78
170	0.19	0.23	0.29	0.40

The Wenzel equation gives a change in the Wenzel contact angle, $\Delta\theta_H^W$, caused by a change in the contact angle on the smooth surface, $\Delta\theta_H$, as

$$\Delta\theta_H^W = r\left(\frac{\sin\theta_e}{\sin\theta_r^W}\right)\Delta\theta_H \tag{14}$$

The gain factor, which is the change in $\cos\theta_r^W$ relative to $\cos\theta_e$ (i.e., the derivative of $\cos\theta_r^W$ with respect to $\cos\theta_e$), is very useful because it separates the idea of the equilibrium contact angle increase occurring by surface topography from the observed contact angle. Using the Wenzel equation we can obtain the Wenzel gain factor as follows:

$$G_e^W = \frac{r\sin\theta_e}{\sin\theta_r^W} \tag{15}$$

Since the effect of roughness is proportional to the radian contact angle changes, the Wenzel gain factor is approximately unity when a contact angle θ_e is close to 90°, but the Wenzel gain factor rapidly increases as the roughness factor increases. Likewise, the CB equation gives a change in the CB contact angle, $\Delta\theta_H^{CB}$, caused by a change in the contact angle on the smooth surface, $\Delta\theta_H$, as

$$\Delta\theta_H^{CB} = (1 - f_2)\left(\frac{\sin\theta_e}{\sin\theta_r^{CB}}\right)\Delta\theta_H \tag{16}$$

Similarly, a CB gain factor, G_e^{CB}, can be obtained by the CB equation as

$$G_e^{CB} = (1 - f_2)\left(\frac{\sin\theta_e}{\sin\theta_r^{CB}}\right) \tag{17}$$

Since $1 - f_2 \leq 1$, $G_e^{CB} \leq 1$. According to McHale, the CB gain factor, G_e^{CB}, is an attenuation of any contact angle hysteresis, while hysteresis increases on a Wenzel-type surface. As a numerical example, if a water droplet is deposited on a rough nylon surface having $\theta_e = 68°$, $\Delta\theta_H = 150°$ and $r = 3$, the apparent contact angle, θ_r^W, will be ~ 0° and thus the contact angle hysteresis on this Wenzel surface, $\Delta\theta_H^W$, will be greater than 150°, i.e., the droplet will be adsorbed onto the rough structure and will not be able to roll off such a hydrophilic rough surface. However, if a water droplet is deposited on a poly(tetrafluoroethylene) (PTFE) having $\theta_e = 120°$, $\Delta\theta_H = 80°$ and $f_2 = 0.74$, the apparent contact angle, θ_r^{CB}, will be 150° and the contact angle hysteresis, $\Delta\theta_H^{CB}$, on this CB surface will be less than 80°, i.e. the surface will become superhydrophobic and liquid droplets will readily roll off at a certain roll-off angle. In the case of dodecane, whose $\theta_e < 90°$ and $\theta_r^{CB} > 90°$, the situation is less favorable, and Equations 16 and 17 cannot be used to predict α of dodecane since the sine curve has a bilateral symmetry with respect to 90°. Hence, Equations 16 and 17 have to be modified for a MS CB surface as

$$\Delta\theta_H^{MS\text{-}CB} = (1 - f_2)\left(\frac{1 + \cos\theta_e}{1 + \cos\theta_r^{CB}}\right)\Delta\theta_H \tag{18}$$

$$G_e^{\text{MS-CB}} = (1 - f_2)\left(\frac{1 + \cos\theta_e}{1 + \cos\theta_r^{\text{CB}}}\right) \quad (19)$$

Hence, if there is a surface having surface properties as shown in Table 2, α can be predicted by Equations 12, 16 and 18.

In Table 2, since the droplet shape begins to deform when m > 10 μL caused by gravity, we use a real R_w, that is, not a value predicted by Equation 13 but a real R_c that has been measured on the surface.

Table 2. Predicted Roll-off Angles of Water and Dodecane on a Very Hydrophobic and Oleophobic Rough Surface.

Parameters	Water on PTFE (CB)		Dodecane on PTFE (metastable CB)	
	50 μL	100 μL	50 μL	100 μL
θ_e (°)	120	120	50	50
$\Delta\theta_H$ (°)	110	110	168	168
f_2	0.74	0.74	0.74	0.74
θ_r^{CB} (°)*	150	150	124	124
$\Delta\theta_H^{CB}$ (°)	50	50	163	163
θ_A^{CB} (°)	180	180	180	180
θ_R^{CB} (°)	30	30	17	17
R_w (mm)	2.5	3.3	3.7	4.5
α (°)	15	10	45	26

* Approximate values if $f_1 + f_2 \sim 1$.

The predicted values of α are 15° and 10° for 50-μL and 100-μL water droplets, and 45° and 26° for 50-μL and 100-μL dodecane droplets, respectively. If liquids having different γ_{LV} are deposited on a solid surface, the roll-off angles of the liquids are strongly influenced by the mass and the surface energy of each liquid.

4.3. Modeling and Preparation of Superhydrophobic and Superoleophobic Woven Fabric

Again, the wettability of a solid surface is determined by two parameters: the chemical composition and the geometrical structure of a rough surface. Therefore, in Part I, we design a MS superoleophobic surface via chemical and geometrical modifications. The surface energy of the fibers is reduced by grafting FS onto nylon and cotton fibers composing NyCo fabric. Macro-scale roughness of the NyCo can be controlled via choice of fabric construction, yarn type (mono- or multifilament (MF)), and fiber diameter. Additionally, micro- and nano-scale roughness on fibers can be achieved by allowing partial condensation of the FS prior to treating the NyCo, thus resulting in deposition of FS particulate condensates over the fiber surface. First, we review how to lower the surface tension of fibers chemically.

4.3.1. Chemical Modification

Lowering surface tension of NyCo begins by grafting low-surface-tension material on the surface of NyCo, such as replicating the FS grafting process developed by Hoefnagels et al., and Stoeber

et al. except that the technique was modified to use microwave radiation in this research. A swatch of NyCo fabric is saturated in a solution containing FS, squeezed at 100 % wet pick-up to remove excess liquid, and cured in a conventional microwave oven at 1250 W, with irradiation times varying from 0 to 60 sec. Whilst the surface energy of NyCo is decreased by FS grafting, silane can form micro- and nano-scale roughness on NyCo and create a high surface area if the FS imparts particulate condensation to the NyCo—the self-condensation of FS will be discussed later in Part I. Such treatment methods correlate easily to a wide variety of textiles that have –OH and –NH groups, such as cotton, polyamides, polyaramids, etc. Fluoroalkyl chains can be attached to the –OH or –NH site via a siloxane or silazane linkage as shown in Figure 4.

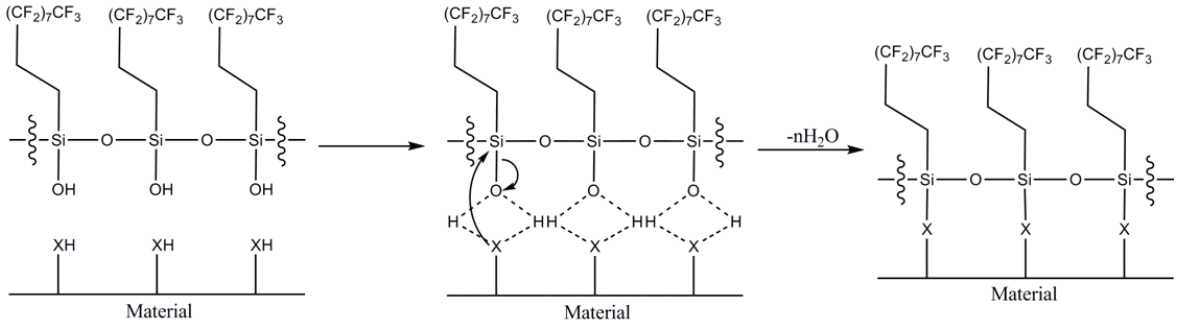

Figure 4. Reaction Mechanism of FS Condensation onto a Surface

where XH is —OH, —SH, —NH—, and —NH_2, etc. Use of microwave radiation in this process greatly enhances the reaction rate of the covalent attachment of silanes to the reactive substrates, as does the presence of acid or base. Since treatment at low pH is avoided for the treatment of cotton and other cellulose derivatives due to the instability of their β-acetal bonds in acidic solutions, this reaction was processed using neutral and basic solutions.

Again, we chemically grafted FS onto a NyCo surface to reduce the surface tension of NyCo and to make the surface less oleophilic. To obtain the Young contact angles for water and dodecane, nylon 6,6 film was treated with FS. The Young contact angles of water on a FS-grafted nylon film were 109º–112º, while the Young contact angles for water on an unmodified nylon surface were 70º–73º. Grafting FS to a nylon film also increased dodecane contact angles. The Young contact angles for dodecane on a FS-grafted nylon film were 73º–75º, while the Young contact angle for dodecane on an unmodified nylon surface was < 5º. The measured values of $\theta_{\text{e-water}}$ and $\theta_{\text{e-dodecane}}$ on FS-treated nylon are critical parameters to consider when designing superoleophobic surfaces using the Wenzel and CB models. FS-grafting onto a nylon film successfully generated a surface having a low surface energy, as shown in Figure 5.

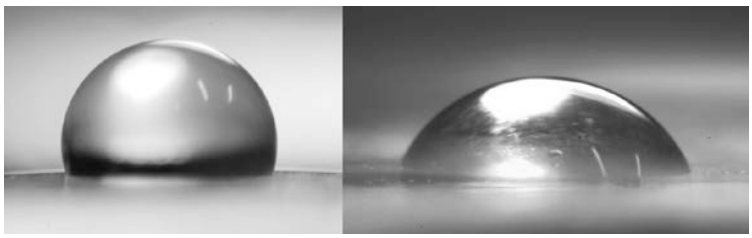

Figure 5. 10-µL Water and Dodecane Droplets on a FS-grafted Nylon Film

4.3.2. Geometrical Modifications

The wetting behavior of a solid surface is also controlled by the geometrical structure of a surface. In this section, we study how to model and modify a rough surface to make the surface highly hydrophobic and oleophobic using plain woven, woven twill, and 3/1 satin woven constructions.

4.3.2.1. Superhydrophobic Oleophobic Plain Woven Structure

To obtain the true surface area we use a flux integral. Figure 6 shows a cross-sectional view of a model of a NyCo plain woven fabric made of monofilament fibers. The distance from the center of a weft (or warp) yarn to the center of an adjacent weft (or warp) yarn is 4*R*; and the distance from the center of a weft (or warp) yarn to the center of an adjacent warp (or weft) yarn is 2*R*. Hence, according to the Pythagorean Theorem, the vector from the center of one weft yarn to the center of an adjacent weft yarn makes a 30° angle to the plane of the fabric.

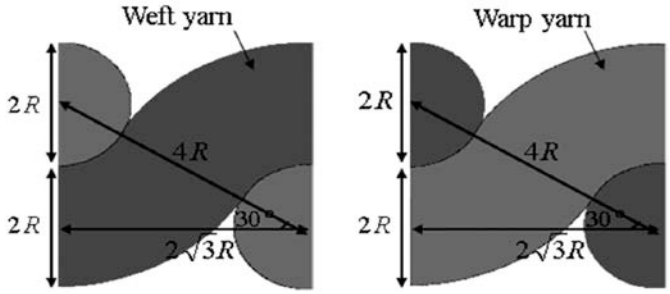

Figure 6. Cross-section Views of a Plain Woven Fabric

Using the flux integral, the area of one yarn in the unit fabric is calculated as

$$r(u,v) = (2R + R\cos v)\cos u\,i + (2R + R\cos v)\sin u\,j + R\cos v\,k \tag{20}$$

$$\left|r_u \times r_v\right| = R(2R + R\cos v) \tag{21}$$

$$A_{\text{yarn in unit area}} = \frac{\int_0^{2\pi}\int_0^{2\pi} R(2R + R\cos v)\,du\,dv}{3} = \frac{8\pi R^2}{3} \tag{22}$$

where *R* is the radius of yarn; *A* is the area; *i*, *j* and *k* are the vectors to *x*-, *y*-, and *z*-axis direction, respectively; *u* and *v* are the notations for the variables of integration. Then, we determine the true fabric surface area as follows:

$$A^{\text{true}}_{\text{fabric}} = \left(2A_{\text{yarn in uynit area}}\right) = 52.64R^2 \tag{23}$$

where $A^{\text{true}}_{\text{fabric}}$ is the intrinsic area of the unit fabric determined by the area of yarn surfaces. The apparent surface area is equal to the area of a plane tangent to the top surface.

$$A^{\text{apparent}}_{\text{fabric}} = \left(2\sqrt{3}R\right)^2 = 12R^2 \tag{24}$$

where $A^{\text{apparent}}{}_{\text{fabric}}$ is the apparent area of the unit fabric shown in Figure 6. Finally, the roughness, r, is

$$r = \frac{52.64R^2}{12R^2} = 4.39 \tag{25}$$

As shown in Equation 25 the plain woven rough surface has high enough r to achieve a MS CB surface.

Next, we look at a plain woven fabric made with MF yarns. Clearly, a MF yarn will have even higher values of r, because the space between the fibers will increase the true surface area while the apparent surface area remains the same. In this case, Equation 23 becomes

$$A^{\text{real}}_{\text{fabric}} = A_{\text{multi}} \approx 52.64R_{\text{y}} \times NR_{\text{f}} \tag{26}$$

Where $A^{real}{}_{fabric}$ is the real area of fabric, A_{multi} is the area of MF yarns, N is the number of filament fibers, R_{y} is the radius of the yarn, and R_{f} is the radius of the filament fibers. Substituting Equation 26 into Equation 25 yields

$$r \approx 4.39\frac{NR_{\text{f}}}{R_{\text{y}}} \tag{27}$$

For example, a plan woven fabric could have $R_{\text{y}} \approx 200$ μm, $N > 50$, and $R_{\text{f}} \approx 10$ μm. Substituting these values into Equation 27 gives $r > 11$. Since $r > 11$ for the MF fabric, we again expect that the surface is adequately rough and that the roughness is composed of the appropriate geometrical structures to be superhydrophobic.

Now, we model a CB plain woven fabric. In Figure 6, the center-to-center distance is $2\sqrt{3}R$ and the contact angle on a CB NyCo surface, $\theta_{\text{r}}^{\text{CB}}$, is defined as

$$\cos\theta_{\text{r}}^{\text{CB}} = \frac{(\pi - \theta_{\text{e}})}{\sqrt{3}}\cos\theta_{\text{e}} + \frac{\sin\theta_{\text{e}}}{\sqrt{3}} - 1 \tag{28}$$

based on Equation 11. Substituting Young contact angles into Equation 28 along with the measured contact angles from the flat nylon film provides $\theta_{\text{r}}^{\text{CB}}$. In addition, if the fabric consists of MF yarns whose $D_{\text{f}} \sim R_{\text{f}}$, as shown in Fig 7, where R_{f} is the fiber radius and $2D_{\text{f}}$ is the distance between two adjacent fibers, the CB contact angle on MF yarn, $\theta_{\text{r}}^{\text{MF}}$, is defined as

$$\cos\theta_{\text{r}}^{\text{MF}} = \frac{(\pi - \theta_{\text{e}})}{2}\cos\theta_{\text{e}} + \frac{1}{2}\sin\theta_{\text{e}} - 1 \tag{29}$$

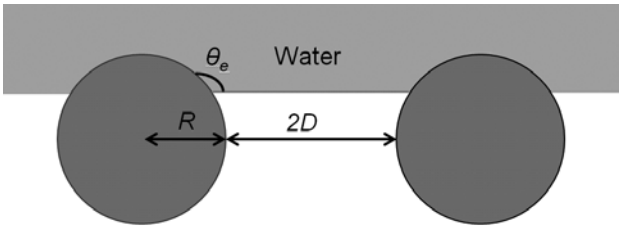

Figure 7. Water Droplet on Two Filament Fibers

For $\theta_e > 90°$, θ_r^{CB} increases with increasing D. For example, if a fabric material is made of PTFE, ($\theta_e = 120°$) and the fibers are closely packed, $\theta_r^{CB} = 131°$; for $D = R$, $\theta_r^{CB} = 146°$; and for $D = 2R$, $\theta_r^{CB} = 152°$ on the MF yarn.

As mentioned above, $109º \le \theta_e$ (water) $\le 112º$ and $73º \le \theta_e$ (dodecane) $\le 75º$ on a surface grafted with FS. By substituting these numbers into Equation 28, we find $133° \le \theta_r^{CB}$ (water) $\le 136°$ and $98° \le \theta_r^{CB}$ (dodecane) $\le 100°$ for the FS-grafted mono-filament plain woven fabric. In the same manner, substituting the same θ_e into Equation 29, we obtain $142° \le \theta_r^{MF}$ (water) $\le 144°$ and $114° \le \theta_r^{MF}$ (dodecane) $\le 115°$ for the FS-grafted MF yarns. Using these values as the effective contact angles for the yarns in the plain woven structure and re-solving Equation 28, i.e., substituting these values into θ_e (water) and θ_e (dodecane) in Equation 28, we predict $161° \le \theta_r^{CB}$ (water) $\le 163°$ and $138° \le \theta_r^{CB}$ (dodecane) $\le 139°$ for the FS-grafted MF plain woven fabric. According to our prediction, properly constructed NyCo MF plain woven fabric can be superhydrophobic and highly oleophobic once the fabric is treated with a low-surface-tension material such as FS.

4.3.2.2. Superhydrophobic Oleophobic Twill Woven Structure

Figure 8 shows a cross-sectional view of a model of a NyCo twill woven fabric made of monofilament fibers. A flux integral can be used to obtain the true area of twill woven fabric as well. The area of one yarn in the unit fabric is

$$A_{\text{yarn in unit area}} = \frac{\int_0^{2\pi}\int_0^{2\pi} R(2R + R\cos v)dudv}{3} + \frac{\pi R^2}{2} = \left(\frac{8\pi^2}{3} + \frac{\pi}{2}\right)R^2 \tag{30}$$

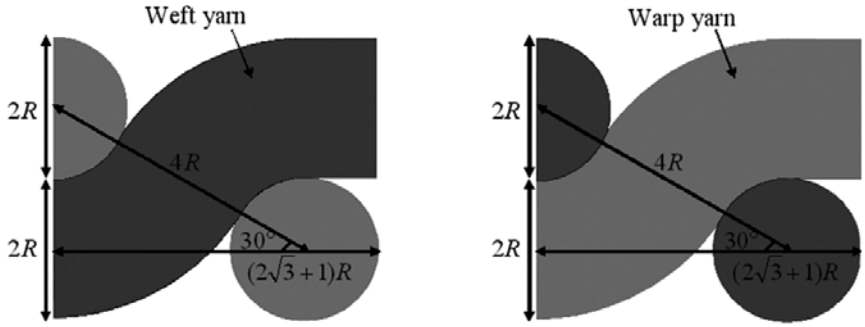

Figure 8. Cross-section View of a Twill Woven Fabric

The area of one yarn in the unit fabric is applied to both weft and warp yarns, and a twill fabric in Figure 8 consists of four yarns in the unit area. Therefore, the true fabric area is:

$$A_{\text{fabric}}^{\text{true}} = 4A_{\text{yarn in unit area}} = 111.56R^2 \tag{31}$$

where $A^{\text{true}}_{\text{fabric}}$ is the intrinsic area of the unit fabric determined by the area of yarn surfaces. The apparent surface area is equal to the area of a plane tangent to the top surface.

$$A_{\text{fabric}}^{\text{apparent}} = \left[R(2\sqrt{3}+1)\right]^2 = 19.93R^2 \tag{32}$$

where $A^{apparent}_{fabric}$ is the apparent area of the unit fabric. Based on Equation 10, the roughness, *r*, is 5.59. If this twill woven fabric is made of yarns having MF fibers as shown in Fig 7, the fabric will have even higher values of roughness and $r > 5.59$, since the space between the fibers will increase the intrinsic surface area while the apparent surface area remains the same. Therefore, *r* of the twill woven rough surface is large enough for it to exist as a MS CB surface regardless of the structure of yarns.

Now, we model a CB twill woven fabric. In Figure 8, the center-to-center distance is $(2\sqrt{3}+1)R$. Thus, $\cos\theta_r^{CB}$ for a CB NyCo surface is defined as

$$\cos\theta_r^{CB} = \frac{4(\pi-\theta_e)+1}{2\sqrt{3}+1}\cos\theta_e + \frac{4\sin\theta_e+1}{2\sqrt{3}+1} - 1 \tag{33}$$

Substituting the same Young contact angles, $109^o \le \theta_e$ (water) $\le 112^o$ and $73^o \le \theta_e$ (dodecane) $\le 75^o$, into Equation 29, we obtain $142° \le \theta_r^{MF}$ (water) $\le 144°$ and $114° \le \theta_r^{MF}$ (dodecane) $\le 115°$ for the FS-grafted MF yarns. Using these values as the effective contact angles for the yarns in the twill woven structure and re-solving Equation 33, i.e., substituting these values into θ_e (water) and θ_e (dodecane) in Equation 33, we predict $150° \le \theta_r^{CB}$ (water) $\le 152°$ and $118° \le \theta_r^{CB}$ (dodecane) $\le 119°$ for the FS-grafted MF twill woven fabric. According to our prediction, properly constructed NyCo MF twill woven fabric can also be superhydrophobic and highly oleophobic once the fabric is treated with a low-surface-tension material such as FS.

4.3.2.3. Superhydrophobic Oleophobic Satin Woven Structure

Figure 9 shows a cross-sectional view of a model of a NyCo 3/1 satin woven fabric made from monofilament fibers. The surface area of a single round monofilament fiber in the unit fabric can be calculated using flux integral to obtain *r* as shown above.

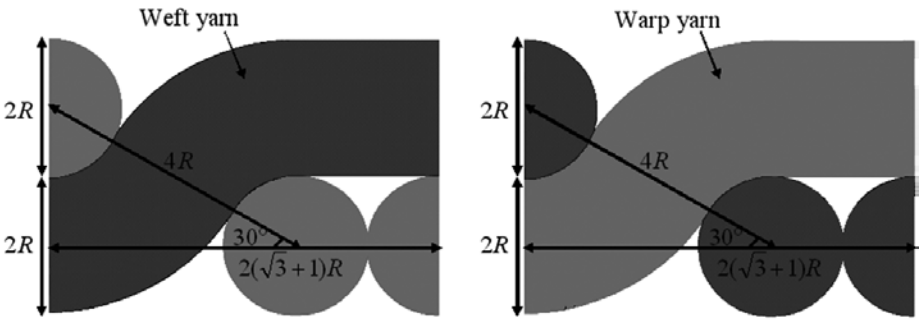

Figure 9. Cross-section View of a 3/1 Satin Woven Fabric

The area of one yarn in the unit fabric is

$$A_{\text{yarn in unit area}} = \frac{\int_0^{2\pi}\int_0^{2\pi} R(2R+R\cos v)\,du\,dv}{3} + \pi R^2 = \left(\frac{8\pi^2}{3}+\pi\right)R^2 \tag{34}$$

The area of one yarn in the unit fabric is applied to both weft and warp yarns, and the satin fabric in Figure 9 consists of six yarns in the unit area. Therefore, the true fabric area is

$$A_{\text{fabric}}^{\text{real}} = 4\text{x}\ A_{\text{yarn in unit area}} = 176.76R^2 \tag{35}$$

where $A^{\text{true}}_{\text{fabric}}$ is the intrinsic area of the unit fabric determined by the area of yarn surfaces. The apparent surface area is equal to the area of a plane tangent to the top surface.

$$A_{\text{fabric}}^{\text{apparent}} = \left[2R(\sqrt{3}+1)\right]^2 = 29.85R^2 \tag{36}$$

where $A^{\text{apparent}}_{\text{fabric}}$ is the apparent area of the unit fabric. Based on Equation 10, the roughness, *r*, is 5.92. If this satin woven fabric is made of yarns having MF fibers as shown in Fig 9, the fabric will have even higher values of roughness and $r > 5.92$, because the space between the fibers will increase the intrinsic surface area while the apparent surface area remains the same. Therefore, the satin woven rough surface has high enough *r* to exist as a MS CB surface regardless of the structure of yarns.

Now, we model a CB 3/1 satin woven fabric. In Figure 9, the center-to-center distance is $(2\sqrt{3}+1)R$. Thus, a CB NyCo surface is defined as

$$\cos\ \theta_{\text{r}}^{\text{CB}} = \frac{2(\pi-\theta_{\text{e}})+1}{\sqrt{3}+1}\cos\theta_{\text{e}} + \frac{2\sin\theta_{\text{e}}+1}{\sqrt{3}+1} - 1 \tag{37}$$

Again, substituting the same Young contact angles above, $109^\circ \le \theta_{\text{e}}$ (water) $\le 112^\circ$ and $73^\circ \le \theta_{\text{e}}$ (dodecane) $\le 75^\circ$, into Equation 29, we obtain $142^\circ \le \theta_{\text{r}}^{\text{MF}}$ (water) $\le 144^\circ$ and $114^\circ \le \theta_{\text{r}}^{\text{MF}}$ (dodecane) $\le 115^\circ$ for the FS-grafted MF yarns. Using these values as the effective contact angles for the yarns in the 3/1 satin woven structure and re-solving Equation 37, we predict $149^\circ \le \theta_{\text{r}}^{\text{CB}}$ (water) $\le 151^\circ$ and $117^\circ \le \theta_{\text{r}}^{\text{CB}}$ (dodecane) $\le 118^\circ$ for the FS-grafted MF 3/1 stain woven fabric. According to our prediction, properly constructed NyCo MF satin woven fabric can also be superhydrophobic and highly oleophobic once the fabric is treated with a low-surface-tension material such as FS.

NyCo MF woven fabric can be superhydrophobic but cannot be superoleophobic by itself, even if the fabric is treated with a low-surface-tension chemical. To achieve superoleophobicity as well as superhydrophobicity, the fabric morphology has to be manipulated by creating bigger spaces between fibers, loosening the fabric structure, or providing more roughness to the surface of NyCo MF fibers. Considering the manufacturing process of woven fabrics, providing more roughness by adding protuberances to the surface of NyCo fibers seems the easiest way to achieve superhydrophobicity and superoleophobicity. Figure 10 shows a NyCo surface covered

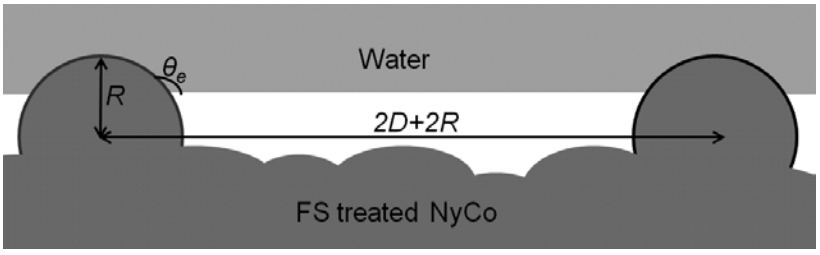

Figure 10. Water Drop on Top of a NyCo fiber Treated in 10% FS Solution Consisting of Base Catalyst

with protuberances in micro and nano size FS. In the next section, we study how to create such a multiscale roughness on the NyCo surface to prepare a MS CB superhydrophobic and superoleophobic woven fabric.

4.3.2.4. Superhydrophobic/Superoleophobic NyCo Woven Fabric

By using FS in conjunction with corrugated, rough surfaces, FS can build multi-scale roughness having low surface energy. Indeed, the previous research presented that the use of condensed silanes increases micro and nano structure corrugation, resulting in increased hydrophobicity and oleophobicity of so-treated cotton. A superhydrophobic and superoleophobic NyCo woven fabric can be developed in the same manner by covalently binding silanes onto the NyCo surface.

Although any soluble base can be an efficient catalyst, we use ammonium hydroxide as a base catalyst to accelerate the displacement of the methoxy or ethoxy substituent, and to facilitate the formation of the corrugated micro- and nanostructure (Fig. 11).

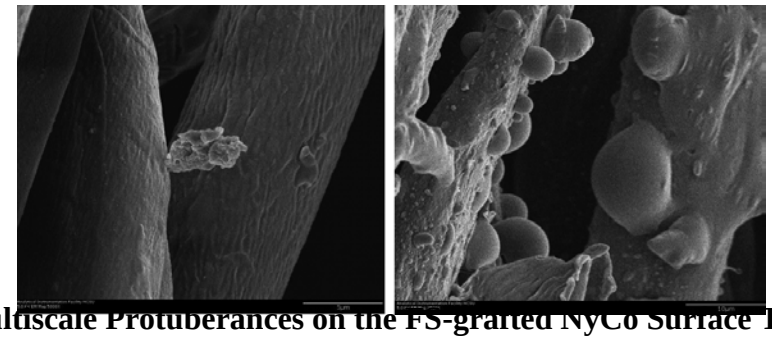

Figure 11. Multiscale Protuberances on the FS-grafted NyCo Surface Treated in 10% Solution of FS with Catalytic Water (left) and 10% FS with NH_4OH (right)

Because FS-treated NyCo without catalytic base has a relatively smooth surface and NyCo treated with FS in the presence of 1% catalytic base has multiscale roughness on the surface, X-ray photoelectron spectra (XPS) of NyCo FS treated both with and without base catalyst were measured and compared with the XPS of untreated NyCo. Table 3 shows the XPS atomic composition of C, N, O, F and Si and the ratio of F/O, F/C and F/Si at the surface of three materials: (a) NyCo treated in a 10% solution of FS with catalytic water, (b) NyCo treated in a 10% solution of FS in the presence of 1% NH_4OH, and (c) untreated NyCo. Both (a) and (b) have almost the same amount of fluorine. However, as shown in Figure 11, NyCo treated in a 10% solution of FS with water exhibits surface morphology very different from (b) although they possess almost the same atomic composition of F and nearly the same values of F/O, F/C and F/Si ratios at the surface. As expected, based on the atomic composition of (c), the untreated NyCo does not have fluorine on the surface.

Table 3. XPS Atomic Composition of FS Treated and Untreated NyCo

Fabric	Atomic composition (%)				Ratio		
	C	O	F	Si	F/O	F/C	F/Si
FS treated NyCo with water	39.1	8	50.2	2.7	6.3	1.3	18.4
FS treated NyCo with NH_4OH	38.4	8.6	50.5	2.5	5.9	1.3	20.4
Control NyCo	77	20.5	0	1.4	0	0	0

By changing FS concentration, curing time, and the number of cures, we can control the morphology of FS protuberances on the NyCo surface and eventually prepare superhydrophobic and superoleophobic woven fabric (Fig. 12). The FS-treated NyCo plain woven fabric shown in Figure 12 is superhydrophobic and superoleophobic. The fabric prevents the absorption of not only water but also dodecane with almost no change of contact angles.

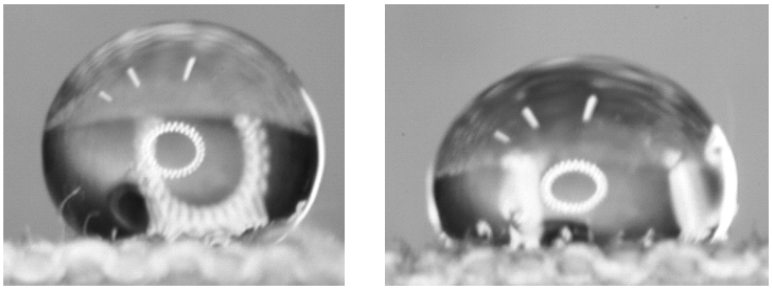

Figure 12. 10-µL Water (left) and Dodecane (right) Droplets on FS-grafted NyCo Plain Woven Fabric Treated via Microwave Synthesis

The FS concentration, curing time, and the number of cures absolutely affect the wetting behavior of FS-treated NyCo woven fabric. This indicates that oil contact angles can be greatly improved by varying such parameters. We suggest that improving the macro-scale geometric morphology of the woven fabric, such as controlling the fiber spacing, manipulating the yarn structure, and choosing the proper woven construction, are also necessary to design and prepare superhydrophobic and superoleophobic fabrics.

4.4. Modeling and Preparation of Superhydrophobic and Superoleophobic Nonwoven Fabric

Superhydrophobic materials are often prepared by applying fluorochemicals to solid surfaces that are naturally rough or by creating new roughness while attaching fluorochemicals. In this study, we compare three different processes for making superhydrophobic and superoleophobic materials, by attaching identical fluoroalkyl chains, $CF_3(CF_2)_7CH_2CH_2$-X, which differ only in the X-group used to attach the fluoroalkyl chain to the surface and the method used to cure the fluoroalkyl materials.

4.4.1. Chemical Modification

4.4.1.1. Pulsed Plasma Polymerization of Fluoroalkyl Acrylates onto Nylon Surface

When perfluoroalkyl acrylates are introduced into plasma, polymerization of the vinyl double bond can be initiated in the vapor phase and on any nearby surfaces. The perfluoroalkyl acrylate polymerization creates a closely packed covering of trifluoromethyl groups on the surface. When this polymerization was carried out in the presence of nylon films, we observed that Young's contact angle for water increased from 70–74° for the untreated nylon film to 123–125° for the plasma-polymerized treatment. Similarly, Young's contact angle for dodecane increased from <5° for the untreated nylon film to 78–81° for the plasma-polymerized treatment as seen in Figures 13 and 14. This demonstrates that a hydrophilic flat nylon surface became hydrophobic upon fluorochemical treatment. At the same time, the oleophilic surface became much less oleophilic, but it did not become oleophobic (i.e. the contact angle for dodecane was still less than 90°).

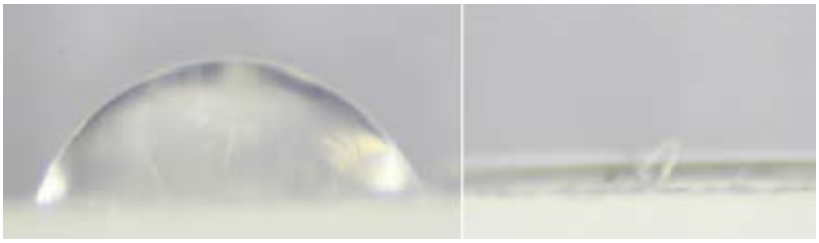

Figure 13. Water (left) and Dodecane (right) Droplets on an Untreated Nylon Film

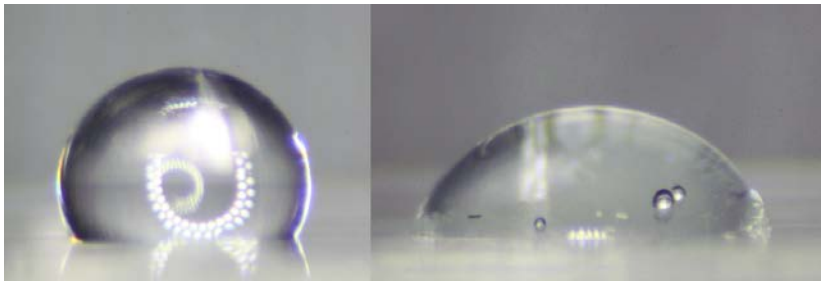

Figure 14. Water (left) and Dodecane (right) Droplets on a Pulse-Plasma-Polymerized PFAC8-grafted Nylon Film
(Source: Lee et al. *Journal of Materials Science*, 2011)

4.4.1.2. Microwave-assisted FS Grafting onto Nylon

Microwave radiation greatly accelerates many reactions, including siloxane condensation. Fluorosiloxanes can self-condense to form nano- or microparticles, which deposit on nearby surfaces. They can also react directly with surfaces and form covalent bonds with them. Thus, they offer great potential to generate a rough, fluorinated surface. For comparison of the effectiveness of the plasma polymerization of fluoroalkyl acrylate to microwave-assisted grafting of fluoroalkylsiloxanes, we applied FS to nylon 6,6 film and used microwaves to assist grafting. Young's contact angles for water on the treated film increased to 124–126° and for dodecane they increased to 70–73° as shown in Figure 15. These results are very close to those above for the plasma-polymerized treatment.

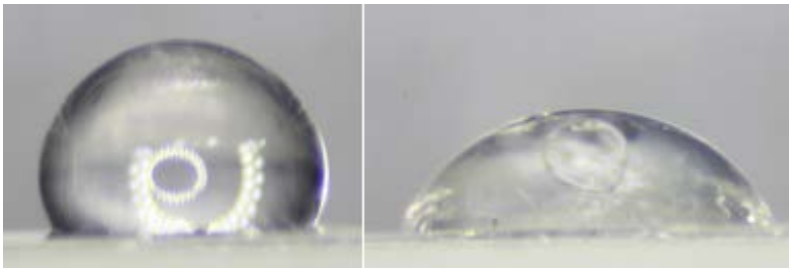

Figure 15. Water (left) and Dodecane (right) Droplets on Microwave-assisted FS-treated Nylon Film

4.4.1.3. FS Grafting onto Nylon via Wet Processing

For comparison to traditional wet processing techniques, FS was applied to a nylon 6,6 film by immersing the film in a solution of FS that was allowed to self-condense and react with the film surface at room temperature. However, the number of reactive groups on the surface of untreated nylon is low. To circumvent this problem, additional sites were added by grafting PAA to the surface followed by condensing EDA with the carboxylic acid groups in PAA. This provided a surface rich in $-NH_2$ groups. After FS deposition on this surface, Young's contact angle for water was 120–124° and for dodecane was 64–68° (Fig. 16). These contact angles are nearly identical to those for the plasma-polymerized fluoroalkyl acrylates. The results of all three methods are shown in Table 4.

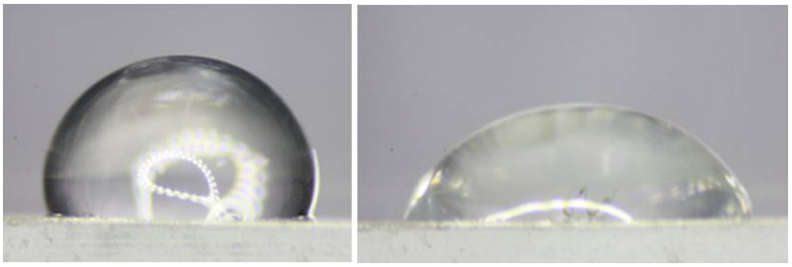

Figure 16. Water (left) and Dodecane (right) Droplets on FS (Wet Processing) Grafted Nylon Film

Table 4. Comparison of Young's Contact Angle of Nylon Films Treated with Fluoroalkyls

Treatment	Contact Angles	
	Water	Dodecane
No treatment	70–74°	<5°
Plasma-polymerized perfluorodecyl acrylate	120–122°	65–67°
Microwave-assisted FS condensation	124–126°	70–73°
Wet processing of FS	120–124°	64–68°

All three methods reduced the surface energy of the nylon film and led to higher contact angles for both water and dodecane. However, none of these treatments resulted in superhydrophobic or oleophobic materials. To accomplish that goal, the surface roughness must be increased. The work reported below uses HNFs to introduce roughness.

4.4.1.4. Comparison of Chemically Modified Fibers

Figures 17 and 18 present SEM images of fibers in an HNF and after treatment with plasma-polymerized PFAC8, microwave-assisted FS, and wet processed FS. At 5000x magnification the wet-processed FS treated sample appears to have fewer protuberances than the fabrics treated via either plasma polymerization or microwave reaction (Fig. 17). Figure 18 shows the rough surface of the three fabrics in greater detail. The plasma-polymerized PFAC8-treated fiber has a sparse distribution of protruding mounds. The microwave-assisted FS-treated fiber shows an undulating surface with crests and depressions. The average distance between two neighboring crests was in the range of 500 nm to 1 µm. In contrast, the wet-processing FS-treated fiber exhibits a very uneven surface with many small protuberances and uniform coverage of the treated fibers. A typical "rocky" structure was observed throughout and the surface appears to have multiple layers of FS condensates. As expected, the surface of untreated fibers is very smooth (Fig. 19).

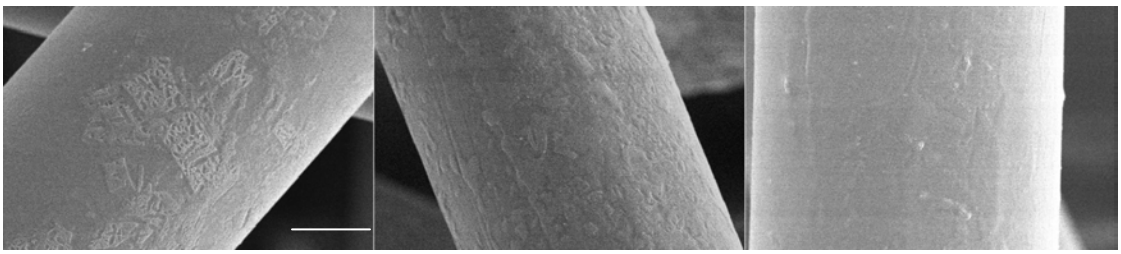

Figure 17. SEM Images of Plasma-Polymerized PFAC8-treated (left); Microwave-assisted FS-treated (center); and Wet-processed FS-treated Fibers in a Nylon Nonwoven (right) (Imaged at 5000x; Bars are 5 μm)

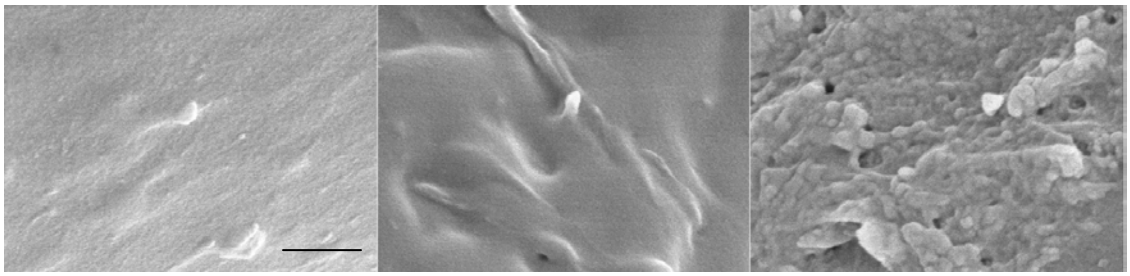

Figure 18. SEM Images of Plasma-Polymerized PFAC8-treated (left); Microwave-assisted FS-treated (center); and Wet-processing FS-treated Fibers in a Nylon Nonwoven (right) (Imaged at 50000x; Bars are 500 nm)

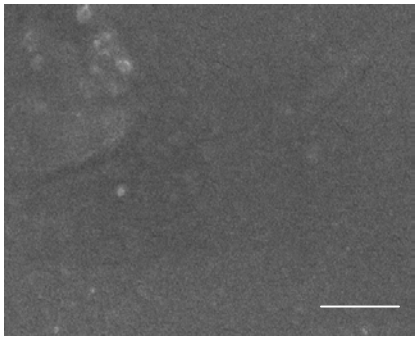

Figure 19. SEM Image of an Untreated Nylon Nonwoven Fiber at 50000X; Bar is 500 nm

4.4.2. Geometrical Modification of Nonwoven Fabric

To create a stable CB surface, Young's contact angle, θ_e, of a liquid residing on a flat surface must be greater than 90°. The surface energy of PFAC8 polymer on a flat glass substrate was determined using the liquid geometric mean method proposed by Fowkes in 1964 and Owens and Wendt in 1969. These authors state that surface tension can be divided into dispersive and polar components. It was found that plasma-polymerized PFAC8 has a very low surface energy (~9 mJ/m^2). Since the surface energies of nonpolar liquids and solids such as dodecane and the PFAC8 plasma polymer are largely determined by the London dispersion forces, we obtain

$$\gamma_L(1+\cos\theta_e = 2\sqrt{\gamma_S^d \cdot \gamma_L^d} = 2\sqrt{\gamma_S \cdot \gamma_L} \quad (38)$$

wherein the superscript d corresponds to the London dispersion force. Substituting γ_s = 9 mJ/m^2 and γ_l = 25.4 mJ/m^2 into Equation38, gives θ_e ~ 79°. Thus the highest contact angle expected for dodecane on a flat, plasma-polymerized-PFAC8 surface is about 80°, far less than the 150° required for superoleophobicity. Similar results are expected for the fluorosiloxane treatments. Therefore, the surface roughness must be increased to attain the higher apparent contact angles needed for superoleophobicity. We achieved this roughness by using a HNF, as shown in Figure 20. We then applied each of the three treatments discussed above to this fabric.

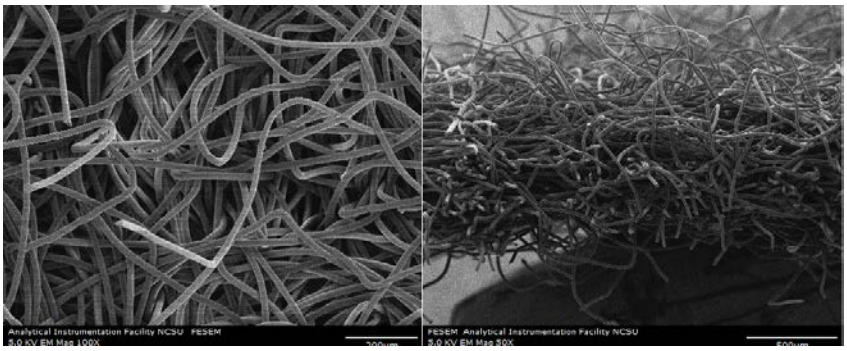

Figure 20. Top View (x100) and Cross-sectional View (x50) of Hydroentangled Nylon Nonwoven Fabric

Despite having a Young's contact angle for dodecane of less than 90°, the PFAC8-plasma-modified nonwoven fabric is both superhydrophobic and superoleophobic, displaying apparent dodecane and water contact angles of 153–155° and 168–171°, respectively (Fig. 21). Similar

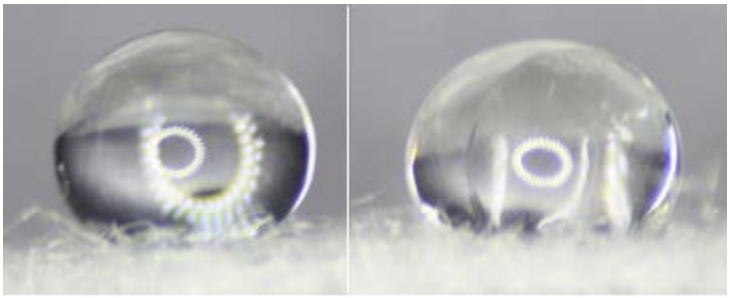

Figure 21. Water (left) and Dodecane (right) Droplets on Plasma-Polymerized PFAC8 on Nylon Nonwoven Fabric

results were achieved for microwave-assisted FS treatment (Fig. 22) and for FS treatment using wet processing (Fig. 23). The measured contact angles for water and dodecane are shown in Table 5. All three treatments give nearly identical contact angles and result in superhydrophobic and superoleophobic materials.

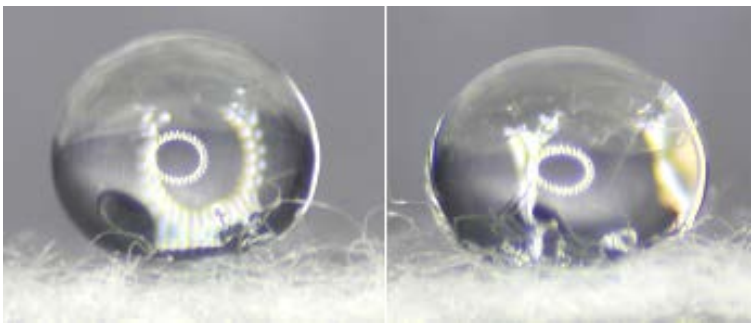

Figure 22. Water (left) and Dodecane (right) Droplets on Microwave-assisted FS Condensation on Hydroentangled Nonwoven Fabric

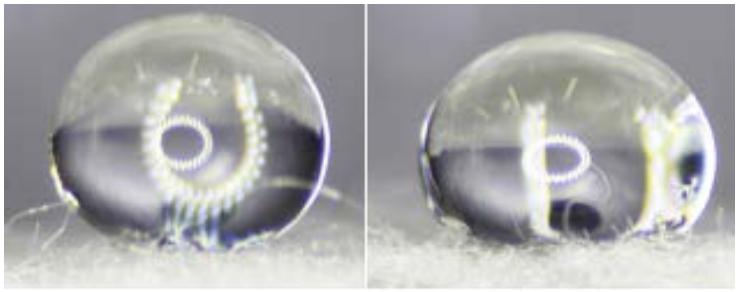

Figure 23. Water (left) and Dodecane (right) Droplets on Hydroentangled Nylon Nonwoven Fabrics FS-condensed via Wet Processing

Table 5. Contact Angles of Water and Dodecane on Treated Hydroentangled Nonwoven Fabrics

Treatment	Contact Angles	
	Water	Dodecane
Plasma-polymerized perfluorodecyl acrylate	168–171°	153–155°
Microwave-assisted FS condensation	172–174°	158–160°
Wet processing of FS	171–173°	154–156°
Predicted from Eq. 41	~180°	155–156°

To better understand the results of Table 5, we modeled the structure of the hydroentangled nonwoven fabric as shown in Figure 24, which represents a cross-sectional view of a liquid droplet sitting on the top layer of the hydroentangled nonwoven fabric. Here, R is defined as the radius of the fiber and $2d$ is the distance between two adjacent fibers.

According to Marmur, the CB model can be rewritten as follows:

$$\cos\theta_{\mathrm{r}}^{\mathrm{CB}} = f r_{\mathrm{f}} \cos\theta_{\mathrm{e}} - 1 + f \tag{39}$$

where f is the fraction of the projected area of the solid surface in contact with the liquid and r_f is the Wenzel roughness in contact with the liquid. (Note that this f is not the same as f_1 in Eq. 11.)

Following Lee and Michielsen and referring to Figure 24, f is given by $R \sin \alpha / (R + d)$ while r_f is $\alpha / \sin \alpha$. According to Marmur, α is equal to $\pi - \theta_e$ when the free energy is a minimum.

Substituting for f and r_f in Equation 11 results in

$$\cos\theta_r^{CB} = \frac{R(\pi - \theta_e)}{d + R}\cos\theta_e + \frac{R}{d + R}\sin\theta_e - 1 \qquad (40)$$

If the apparent contact angle is given by Equation 40, the drop will exhibit stable CB behavior. However, if the apparent contact angle is given by Equation 11, but Equation 40 is not satisfied, the drop will be in the MS CB state. On closer examination of Equation 39, we note that r_f and f are both positive, r_f is greater than 1 and f is less than 1. Therefore, if $\theta_e < 90°$, θ_r^{CB} can be >150° only if f is very small (the fibers are very far apart) or if the liquid is in the MS CB state.

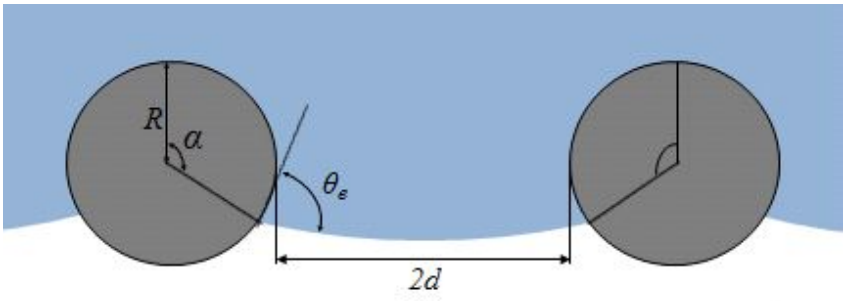

Figure 24. Liquid Droplet Depicted Sitting on top of a Superhydrophobic/Superoleophobic Surface

R is the radius of a fiber, $2d$ is the spacing between two adjacent fibers along the liquid–air interface line, α is the fraction of the circle between vertical and the liquid contact point and θ_e is Young's contact angle. (Source: Lee et al. *Journal of Materials Science*, 2011)

The pore ratio of the top layer of hydroentangled nonwoven fabric in Figure 20 is calculated to be 93% ($f_2 \sim 0.93$), where the pore ratio is

$$\text{pore ratio} = f_2 = 1 - \frac{\text{area occupied by fibers}}{\text{total area}} \qquad (41)$$

Because f_2 of Equation 11 is equal to $1 - (R \sin\theta_e / (d + R))$ from Equation 40, after substituting $R \sim 10$ µm and $65° \leq \theta_{e\text{-dodecane}} \leq 67°$ into f_2, the average value of d can be calculated: 119 µm $\leq d \leq$ 121 µm. Then, substituting R, d, and θ_e into Equation 40 results in $150° \leq \theta_{r\text{-dodecane}} \leq 151°$ and $\theta_{r\text{-water}} \sim 180°$. As shown in Table 5, the measured contact angles for all three treated fabrics are in good agreement with the predicted values.

All three treatments resulted in nearly the same contact angle on flat films. In addition, the measured contact angles for all three treatments are well represented by Equation 11 considering only the fabric structure and not the nanostructures on the fiber surfaces. This means that the fabric structure and the surface energy of the fluorochemicals are the dominant factors determining whether the material will be superhydrophobic and superoleophobic. The

nanostructures observed on the fibers appear to play no role in the apparent contact angles of these materials.

Another method for distinguishing between these treatments is to examine the roll-off angles for liquid droplets. The roll-off angles of water and dodecane were measured by placing the treated nonwoven fabric on a level platform mounted on a rotation stage and inclining the fabric (Table 6). The advancing and the receding contact angles were measured and the roll-off angles were recorded when the droplet began to move. The contact angle hysteresis (CAH)—the difference between the advancing and the receding contact angles—determines how easily a drop rolls off the surface of the fabric. (Figs. 25 and 26.) The advancing contact angles, θ_A, for both water and dodecane were ~180° for all three surfaces when the droplets began to roll off our superhydrophobic/ superoleophobic surfaces. It was observed that the receding contact angles, θ_R, of water on the treated nonwoven fabrics were 145 – 155° whereas for dodecane $\theta_R < 30°$ on the same fabric. The roll-off angles also depend on the weight of the droplet and the surface tension of the liquid since $mg \sin\alpha \approx \gamma_L D (\cos\theta_R - \cos\theta_A)$ where m is the mass of the droplet, g is the gravitational acceleration, α is the roll-off angle, γ_L is the liquid surface tension, and D is the contact diameter of the droplet on the surface. Although the roll-off angles of a 50-µL droplet of water and dodecane on the treated nonwoven surface were 21° and 36°, respectively, as shown in Figures 25 and 26, if the drop volume is reduced to 10 µL, the drops do not roll off the surface even if the fabric is tilted to the vertical position (90°). This demonstrates a direct correlation between the weight of the droplet and its roll-off angle.

Table 6. Roll-off Angles for Different Treatments on Nylon Nonwoven

Treatment	Roll-off angles	
	Water	Dodecane
Plasma-polymerized perfluorodecyl acrylate	9–11°	26–29°
Microwave-assisted FS condensation	6–8°	21–24°
Wet processing of FS	8–10°	25–28°

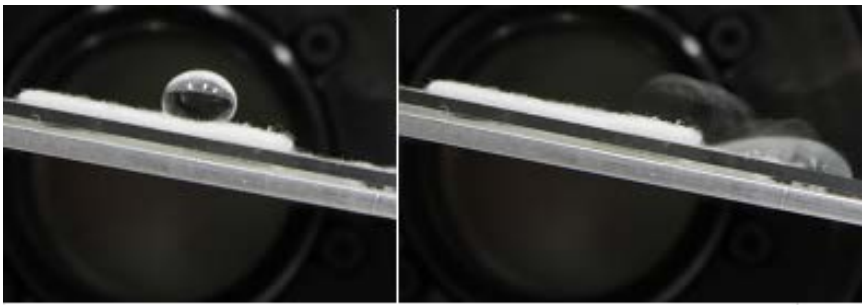

Figure 25. Water Rolling Off a Superhydrophobic/Superoleophobic Surface

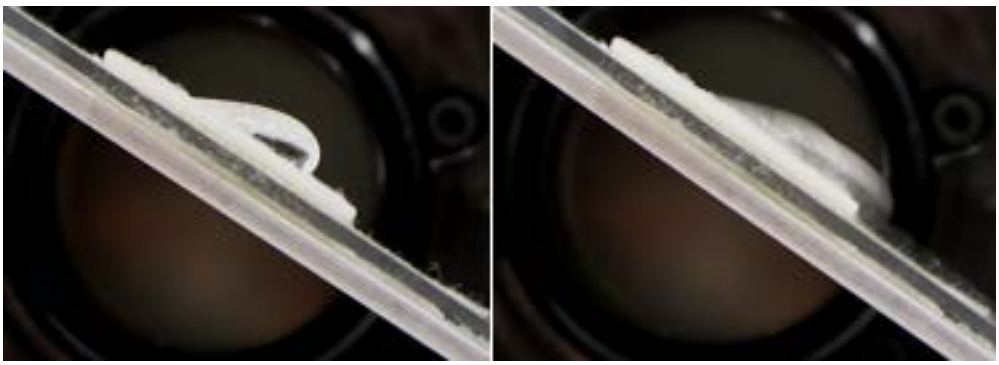

Figure 26. Dodecane Rolling Off a Superhydrophobic/Superoleophobic Surface

4.4.3. Anti-icing Properties of Superhydrophobic Superoleophobic Nonwoven Surface

The anti-icing properties of microwave-assisted FS-grafted superhydrophobic/ superoleophobic nylon nonwoven fabric have been observed and compared to a control fabric. The series of pictures below show the difference in the behavior between a superhydrophobic nonwoven fabric and a control fabric (Figs. 27 and 28).

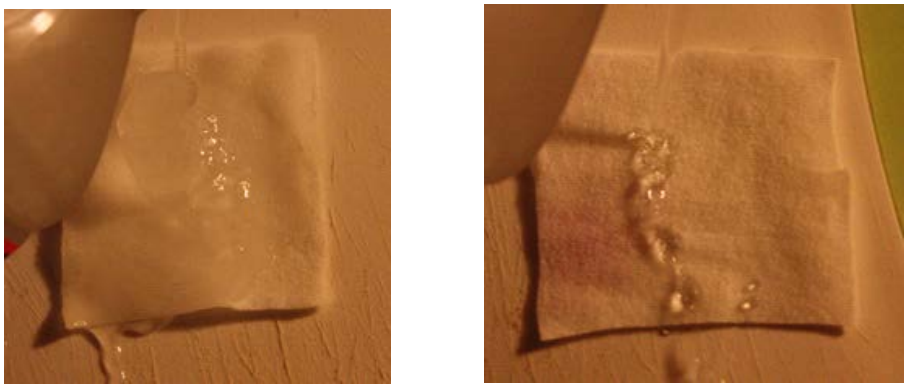

Figure 27. Ice Formation Visible on the Untreated Nylon Nonwoven Fabric (left) and Supercooled Water on FS-treated Superhydrophobic Nylon Nonwoven Fabric (right)

Figure 28. Ice Formed on the Untreated Fabric (left) and No Visible Ice on the FS-treated Fabric (right)

The supercooled water was dropped on both the untreated nylon nonwoven fabric and the FS treated superhydrophobic nylon nonwoven fabric. As the droplets from the bottle fell on the untreated fabric it immediately formed ice on the surface and, as the droplets continued to fall, the ice build-up increased. This can be attributed to the fact that the untreated nylon nonwoven fabric is hydrophobic and absorbed the supercooled water. This facilitated the crystallization of water, converting it into ice. In the case of superhydrophobic nylon nonwoven fabric, the supercooled water was not absorbed into the fabric and the nucleation process did not occur, preventing the formation of ice. Since the fabrics were placed on an inclined plane, a similar experiment was carried out when the fabrics were kept on a flat surface to understand the influence of inclination on anti-icing.

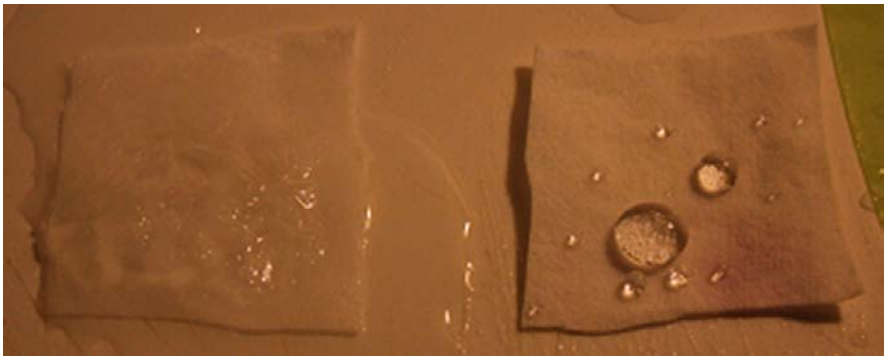

Figure 29. Ice Present on Untreated Nylon Nonwoven (left) and No Visible Ice on FS-treated Superhydrophobic Nylon Nonwoven (right) Placed on a Flat Surface

Figure 29 shows ice present on the untreated nylon nonwoven fabric and no ice formation on FS treated superhydrophobic nonwoven fabric. Thus, the anti-icing property of the fabrics was not influenced by the inclination of the fabrics. The experiment was also carried out on untreated and FS-treated nylon films (Fig. 30). Ice formation was observed on both the films. This shows that roughness is necessary to exhibit anti-icing. The anti-icing property follows the same mechanism as superhydrophobicity. For a rough surface (nylon nonwoven) there are more air-pockets than on a smooth surface (film), which prevents water from getting into the fabric and turning into ice.

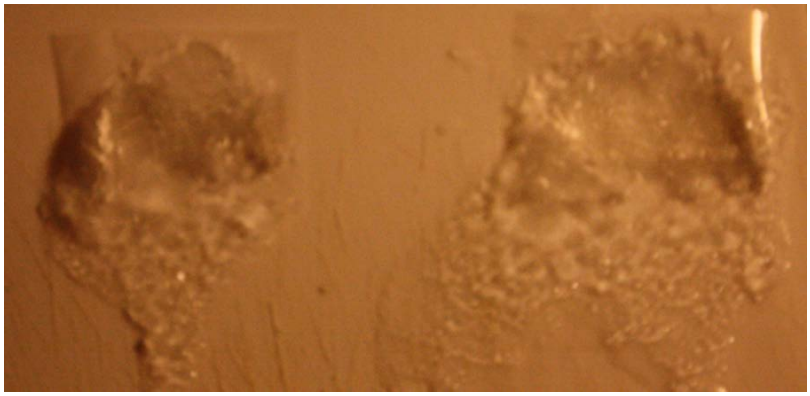

Figure 30. Ice Present on Both Untreated (left) and FS-treated Nylon Films (right)

5. CONCLUSION

In the first part of this report, we studied how to create superhydrophobic and superoleophobic woven fabrics. A superhydrophobic superoleophobic surface is obtained by two criteria: low surface tension and a properly designed rough surface having appropriate surface roughness and morphology. To make woven fabric superhydrophobic and superoleophobic, NyCo MF plain woven fabric was treated with FS which has a very low surface tension and provides more roughness to the fabric by generating micro and nano-size protuberances in the form of FS condensates on the fiber surfaces. From the Young contact angles of water and dodecane on a FS-grafted nylon film, we could predict the apparent contact angles on FS-grafted NyCo MF plain, twill, and 3/1 satin woven fabrics. Forming multiscale geometric structure on the NyCo was also important to improve hydrophobicity and oleophobicity of the fabric, and consequently this treatment resulted in a highly hydrophobic and oleophobic woven fabric material. Finally, superhydrophobic superoleophobic plain woven fabric has been prepared using the Wenzel and the CB equations. Although superoleophobicity is achieved via the MS CB model, the fabric can prevent the absorption of oil as well as water with almost no change of contact angles.

In the second part of this report, three methods for preparing superhydrophobic/ superoleo-phobic/ anti-icing hydroentangled nonwoven fabrics were carefully studied: pulse plasma polymerization of PFAC8, microwave-assisted fluorosiloxane condensation, and fluorosiloxane condensation via wet processing. The apparent contact angles and roll-off angles for water and dodecane droplets were measured. Although the surface morphology of the fibers treated in each process were quite different, the apparent contact angles were nearly the same, up to 174° for water and 160° for dodecane. In addition, roll-off angles as low as 6° for water and 21° for dodecane were obtained for a 50-μL droplet volume. On the other hand, 10-μL droplets of water and dodecane did not roll off any of the surfaces.

Modeling the behavior of liquids on the fluorochemical-treated HNF showed that the influence of nanoparticle structures on the apparent contact angles was insignificant. The two controlling parameters were the low surface energy imparted by either of the fluorochemicals used and the structure of the nonwoven fabric (fiber size and spacing).

Supercooled water was poured onto a frozen superhydrophobic surface, a microwave-associated fluorosilane-grafted nylon nonwoven fabric, to demonstrate the anti-icing properties of superhydrophobic surfaces. Supercooled water was also poured onto a fluorosilane-grafted nylon film; the water built ice as it did on a frozen untreated film. This indicates that chemical coating is not enough to develop anti-icing surfaces but proper roughness is required, i.e. the air-pockets between protuberances of a superhydrophobic rough surface seem to reduce the total contact area between supercooled water and the fabric surface, and that results in the prevention of ice crystallization on the fabric surface.

6. REFERENCES

Balkenede, A. R, Boogaard, H. J. A. P. van de, Scholten, M., Willard, N. P. (1998), "Evaluation of different approaches to assess the surface tension of low-energy solids by means of contact angle measurements," *Langmuir*, 14, 5907-5912.

Barton, A. F. M. (1983), *CRC Handbook of solubility parameters and other cohesion parameters*, Boca Raton, CRC Press, Inc.

Barthlott, W., Neihuis, C. (1997), "Purity of the sacred lotus, or escape from contamination in biological surfaces," *Planta*, 202, 1-8.

Bico, J., Tordeux, C., Quere, D. (2001), "Rough wetting," *Europhys Lett*, 55, 214-220.

Brar, T., France, P., Smirniotis, P. (2001), "Heterogeneous versus homogeneous nucleation and growth of zeolite A," *J Phys Chem B*, 105, 5383-5390.

Chhowalla, M., Amaratunga, G. A. J., Milne, W. I., McKinley, G. H., Gleason, K. K. (2003), " Superhydrophobic carbon nanotube forests," *Nano Lett*, 3, 1701-1705.

Fowkes. F. M. (1963), "Additivity of intermolecular forces at interfaces: I. Determination of the contribution to surface and interfacial tensions of dispersion forces in various liquids," *J Phys Chem*, 67, 2538-2541.

Fuerstner, R., Barthlott, W., Neinhuis, C., Walzel, P. (2005), "Wetting and self-cleaning properties of artificial superhydrophobic surfaces," *Langmuir*, 21, 956-961.

Han, J. T., Xu, X., Cho, K. (2005), "Diverse access to artificial superhydrophobic surfaces using block copolymers," *Langmuir*, 21, 6662-6665.

Hayn, R., Owens, J., Boyer, S., McDonald, R., Lee, H. (2011), "Preparation of highly hydrophobic and oleophobic textile surfaces using microwave-promoted silane coupling," *Journal of Materials Science*, 46, 2503-2509.

Hoefnagels, H., Wu, D., With, G., Ming, W. (2005), "Biomimetic superhydrophobic and highly oleophobic cotton textiles," *Langmuir*, 23, 13158-13163.

Jopp, J., Gruell, H., Yerushalmi-Rozen, R. (2004), "Wetting behavior of water droplets on hydrophobic microtextures of comparable size," *Langmuir*, 20, 10015-10019.

Kim, J., Kim, C. (2002), "Nanostructured surfaces for dramatic reduction of flow resistance in droplet-based microfluidics," *J Microelectromechanical Systems*, 11(5), 454-464.

Kim, S. H., Kim, J., Kang, B., Uhm, H. (2005), "Superhydrophobic CF_x coating via in-line atmospheric RF plasma of He–CF_4–H_2," *Langmuir*, 21, 12213-12217.

Kovats, E. (1989), "Wetting of low energy model surfaces," *Pure and App Chem*, 61, 1937-1944.

Krevelen, D. W. van, Hoftyzer, P. J. (1980), *Properties of Polymers*, New York, Elsvier/North-Holland Inc.

Krupenkin, T. N., Taylor, J. A., Schneider, T. M., Yang, S. (2004), "From rolling ball to complete wetting: The dynamic tuning of liquids on nanostructured surface," *Langmuir*, 20, 3824-3827.

Kwong, V. H., Mossman, M. A., Whitehead, L. A. (2004), "Control of reflectance of liquid droplets by means of electrowetting," *App Optics*, 43(4), 808-813.

Lau, K. K. S., Bico, J., Teo, K. B. K., Chhowalla, M., Amaratunga, G. J., Milne, W. I., McFinley, G. H., Gleason, K. K. (2003), "Superhydrophobic carbon nanotube forests," *Nano Lett.*, 3, 1701-1705.

Lee, H., Michielsen, S. (2006), "Lotus effect: superhydrophobicity," *Journal of Textile Institute*, 97, 455-462.

Lee, H., Owens J. (2010), "Design of superhydrophobic ultraoleophobic NyCo," *Journal of Materials Science*, 45, 3247-3253.

Lee, H., Owens J. (2011), "Motion of liquid droplets on a superhydrophobic oleophobic surface," *Journal of Materials Science*, 46, 69-76.

Liu, H., Feng, L., Zhai, J., Jiang, L., Zhu, D. (2004), "Reversible wettability of a chemical vapor deposition prepared ZnO film between superhydrophobicity and superhydrophilicity," *Langmuir*, 20, 5659-5661.

Marmur, A. (2004), "The Lotus effect: superhydrophobicity and metastability," *Langmuir*, 20, 3517-3519.

McHale, G., Shirtcliffe, N. J., Newton, M. I. (2004), "Contact-angle hysteresis on super-hydrophobic Surfaces," *Langmuir*, 20, 10146-10149.

Miwa, M., Nakajima, A., Fujishima, A., Hashimoto, K., Watanabe, T. (2004), "Effects of the surface roughness on sliding angles of water droplets on superhydrophobic surfaces," *Langmuir*, 16, 5754-5760.

Nakajima, A., Hashimoto, K., Watanabe, T. (2005), "Transparent superhydrophobic thin films with self-cleaning properties," *Langmuir*, 16, 7044-7047.

Ostrovskaya, L., Podesta, A., Milani, P., Ralchenko, V. (2003), "Influence of surface morphology on the wettability of cluster-assembled carbon films," *Europhys Lett*, 63(3), 401-407.

Otten, A., Herminghaus, S. (2004), "How plants keep dry: A physicist's point of view," *Langmuir*, 20, 2405-2408.

Pal, S. Weiss, H., Keller, H., Mueller-Plathe, F. (2005), "Effect of nanostructure on the properties of water at the water–hydrophobic interface: a molecular dynamics simulation," *Langmuir*, 21, 3699-3709.

Patankar, N. A. (2003), "On the modeling of hydrophobic contact angles on rough surfaces," *Langmuir*, 19, 1249-1253.

Roura, P., Fort, J. (2002), "Comment on "Effects of the surface roughness on sliding angles of water droplets on superhydrophobic surfaces," *Langmuir*, 18, 566-569.

Sun, M., Luo, C., Xu, L., Ji, H., Ouyang, Q., Yu, D., Chen, Y. (2005), "Artificial lotus leaf by nanocasting," *Langmuir*, 21, 8978-8981.

Sun, T., Feng, L., Gao, X., Jiang, L. (2005), "Bioinspired surfaces with special wettability," *Acc Chem Res*, 38, 644-652.

Tadanaga, K., Morinaga, J., Matsuda, A., Minami, T. (2000), "Superhydrophobic-superhydrophilic micropatterning on flowerlike alumina coating film by the sol–gel method," *Chem Mater*, 12, 590-592.

Yoshimitsu, Z., Nakajima, A., Watanabe, T., Hashimoto, K. (2002), "Effects of surface structure on the hydrophobicity and sliding behavior of water droplets," *Langmuir*, 18, 5818-5822.

Zhai, L., Cebeci F. C., Robert E. C., Rubner M. F. (2004), “Stable superhydrophobic coatings from polyelectrolyte multilayers,” *Nano Lett*, 4, 1349-1353.

Zhang, X., Sato, O., Taguchi, M., Einaga, Y., Murakami, T., Fujishima, A. (2005), “Self-cleaning particle coating with antireflection properties,” *Chem Mater*, 17, 696-700.

LIST OF SYMBOLS, ABBREVIATIONS, AND ACRONYMS

$A^{apparent}$	apparent area of the unit fabric
AFRL	Air Force Research Laboratory (AFRL)
A^{true}	intrinsic area of the unit fabric
CB	Cassie–Baxter
D_f	half the distance between two adjacent fibers
Dstl	UK Defense Science and Technology Laboratory
FS	1H,1H,2H,2H-perfluorodecyltrimethoxysilane
f_1	surface area of liquid in contact with the solid divided by the projected area
f_2	surface area of liquid in contact with air trapped in pores of rough surface, divided by the projected area
G_e^{CB}	Cassie–Baxter gain factor,
G_e^{W}	Wenzel gain factor
g	gravitational acceleration
HN	hydroentangled nylon
HNF	hydroentangled nylon nonwoven fabric
MF	multifilament (yarn)
MS	metastable
m	mass
N	number of filament fibers in a yarn
NyCo	nylon–cotton woven fabric
PFAC8	1H,1H,2H,2H-perfluorodecyl acrylate
PTFE	poly(tetrafluoroethylene)
R	radius of yarn
RD&EC	Natick Soldier Research, Development, and Engineering Center
RF	radio frequency
R_c	radius of wetting area measured on a surface
R_f	radius of filament fibers
R_w	radius of the wetting area on a surface (generally a predicted value)
R_y	radius of yarn
r	roughness; total wet area of rough surface/apparent surface area in contact with a liquid droplet
SEM	scanning electron microscope
W_{SL}^{a}	thermodynamic work of adhesion,
α	roll-off angle of a droplet on a smooth surface
$\Delta\theta_H$	contact angle hysteresis, the difference between θ_A and θ_R
γ^d	London dispersion forces at an interface (LV, SL or SV)
γ^H	intermolecular forces at the interface caused by hydrogen bonds
γ^{ind}	intermolecular forces at the interface caused by induced dipoles
γ_{LV}	surface tension at the liquid–vapor interface
γ^m	intermolecular forces at the interface caused by metallic interaction
γ^p	intermolecular forces at an interface caused by permanent dipoles
γ_{SL}	surface tension at the solid–liquid interface
γ_{SV}	surface tension at the solid–vapor interface
θ_A	advancing contact angle

θ_e	droplet–surface contact angle
θ_H	liquid contact angle on a smooth surface
θ_R	receding contact angle
θ_r^{CB}	liquid contact angle on a rough surface (by Cassie–Baxter approach)
θ_r^{MF}	Cassie–Baxter contact angle on multifilament yarn
θ_r^{W}	liquid contact angle on a rough surface (by Wenzel's approach)